remote sensing

MDPI

Article

Evaluating Different Crown Reconstruction Approaches from Airborne LiDAR for Quantifying APAR Distribution Using a 3D Radiative Transfer Model

Xun Zhao [1,2], Can Liu [1,*], Jianbo Qi [3], Lijuan Yuan [2], Zhexiu Yu [2], Siying He [2] and Huaguo Huang [2]

[1] Chongqing Ecological and Environmental Monitoring Center, Chongqing 401147, China; xunzhao@bjfu.edu.cn
[2] State Forestry and Grassland Administration Key Laboratory of Forest Resources and Environmental Management, Beijing Forestry University, Beijing 100083, China; lj_yuan2021@bjfu.edu.cn (L.Y.); yzhexiu@bjfu.edu.cn (Z.Y.); siyinghe@bjfu.edu.cn (S.H.); huaguo_huang@bjfu.edu.cn (H.H.)
[3] Innovation Research Center of Satellite Application, Faculty of Geographical Science, Beijing Normal University, Beijing 100875, China; jianboqi@bnu.edu.cn
* Correspondence: lc_cqee@126.com

Abstract: Accurately quantifying fine-scale forest canopy-absorbed photosynthetically active radiation (APAR) is essential for monitoring forest growth and understanding ecological processes. The development of 3D radiative transfer models (3D RTMs) enables the precise simulation of canopy–light interactions, facilitating better quantification of forest canopy radiation dynamics. However, the complex parameters of 3D RTMs, particularly detailed 3D scene structures, pose challenges to the simulation of radiative information. While high-resolution LiDAR offers precise 3D structural data, the effectiveness of different tree crown reconstruction methods for APAR quantification using airborne laser scanning (ALS) data has not been fully investigated. In this study, we employed three ALS-based tree crown reconstruction methods: alphashape, ellipsoid, and voxel-based combined with the 3D RTM LESS to assess their effectiveness in simulating and quantifying 3D APAR distribution. Specifically, we used two distinct 3D forest scenes from the RAMI-V dataset to simulate ALS data, reconstruct virtual forest scenes, and compare their simulated 3D APAR distributions with the benchmark reference scenes using the 3D RTM LESS. Furthermore, we simulated branchless scenes to evaluate the impact of branches on APAR distribution across different reconstruction methods. Our findings indicate that the alphashape-based tree crown reconstruction method depicts 3D APAR distributions that closely align with those of the benchmark scenes. Specifically, in scenarios with sparse (HET09) and dense (HET51) canopy distributions, the APAR values from scenes reconstructed using this method exhibit the smallest discrepancies when compared to the benchmark scenes. For HET09, the branched scenario yields RMSE, MAE, and MAPE values of 33.58 kW, 33.18 kW, and 40.19%, respectively, while for HET51, these metrics are 12.74 kW, 12.97 kW, and 10.27%. In the branchless scenario, HET09′s metrics are 10.65 kW, 10.22 kW, and 9.79%, and for HET51, they are 2.99 kW, 2.65 kW, and 2.11%. However, differences remain between the branched and branchless scenarios, with the extent of these differences being dependent on the canopy structure. Our conclusion demonstrated that among the three tree crown reconstruction methods tested, the alphashape-based method has the potential for simulating and quantifying fine-scale APAR at a regional scale. It provides a convenient technical support for obtaining fine-scale 3D APAR distributions in complex forest environments at a regional scale. However, the impact of branches in quantifying APAR using ALS-reconstructed scenes also needs to be further considered.

check for updates

Academic Editor: Jochem Verrelst

Received: 29 October 2024
Revised: 14 December 2024
Accepted: 19 December 2024
Published: 27 December 2024

Citation: Zhao, X.; Liu, C.; Qi, J.; Yuan, L.; Yu, Z.; He, S.; Huang, H. Evaluating Different Crown Reconstruction Approaches from Airborne LiDAR for Quantifying APAR Distribution Using a 3D Radiative Transfer Model. *Remote Sens.* **2025**, *17*, 53. https://doi.org/10.3390/rs17010053

Copyright: © 2024 by the authors. Licensee MDPI, Basel, Switzerland. This article is an open access article distributed under the terms and conditions of the Creative Commons Attribution (CC BY) license (https://creativecommons.org/licenses/by/4.0/).

Keywords: airborne laser scanning; 3D radiative transfer model; quantifying; absorbed photosynthetically active radiation (APAR)

1. Introduction

Absorbed photosynthetically active radiation (APAR) represents the solar radiation absorbed by vegetation in the photosynthetically active radiation region (400–700 nm) [1]. As the primary energy source for photosynthesis, APAR is directly related to vegetation growth and is thus widely used to quantify and assess vegetation productivity and monitor growth status [2]. Furthermore, APAR is a key parameter for the exchange of energy, materials, and momentum between vegetation, the atmosphere, and the biosphere [3,4]. It reflects the light use efficiency (LUE) of vegetation and reveals the dynamic interactions between vegetation and its surrounding environment [5]. In ecological process models, APAR is an important input variable, essential for quantifying and understanding energy exchanges, carbon and water cycles, and biogeochemistry of terrestrial ecosystems [6]. Therefore, accurately quantifying the distribution of APAR in complex vegetation canopies is of great significance for understanding ecological processes and meeting the needs of various ecological applications.

However, effectively quantifying APAR distribution in forest canopies is challenging due to the spatiotemporal variability of light, the complexity of forest structure, and their radiative interaction mechanisms [7]. Traditional methods primarily use quantum sensors and optical instruments to measure APAR in vegetation canopies [8]. These methods commonly focus on stand-scale measurements, which are time-consuming and labor-intensive, making it difficult to meet the demand for detailed APAR measurements at the tree or leaf level [9]. Although some current global ecological process models (e.g., LPJ [10], SiB3 [11]) with coarse resolution are available to quantify the distribution of light, their assumptions of simplified vegetation canopies ignore the horizontal and vertical structural heterogeneity of vegetation. This presents a challenge for accurately quantifying APAR distribution in vegetation canopies and fails to meet the need for detailed characterization of APAR distribution in canopies.

With the rapid advancement of computer technology, 3D radiative transfer models (3D RTMs) based on real scenes, such as DART [12] and LESS [13,14], have garnered increasing attention from researchers. These models are widely employed in various tasks, including validating physical models [15], inversion algorithm validation [16,17], evaluation of vegetation indices [18], developing sensor missions [19], and analyzing signal sensitivity [20]. Due to their ability to intricately characterize the radiation transfer process between photons and canopy structures, 3D radiative transfer models provide a convenient technical tool for accurately depicting the radiation distribution in complex forest canopies. In the past, researchers have also utilized these models to quantify the light distribution in complex forest canopies [7,9], providing reliable data support for understanding ecological processes and meeting the demands of precision forest management. However, the numerous and complex input parameters of 3D RTMs, particularly accurate structural parameters, remain the primary constraints on their further development and widespread application.

Currently, due to its ability to accurately obtain 3D information on vegetation canopy structure, LiDAR technology is increasingly being used by researchers as a crucial data source for input into 3D RTMs to parameterize 3D scenes [19,21,22]. Terrestrial laser scanning (TLS) point clouds with plot-scale provide more detailed structural information (e.g., branches and trunks), enabling the precise reconstruction of explicit forest scenes, researchers have widely combined TLS with 3D RTMs for accurate radiation information

simulation [23,24]. In contrast, research on using airborne laser scanning (ALS) point clouds with regional-scale capture capability for reconstructing 3D scenes and quantifying the distribution of APAR in complex canopies remains inadequately investigated. Specifically, tree crown reconstruction from ALS point clouds currently predominantly employs three methods: alphashape-based [13], ellipsoid-based [25], and voxel-based [26]. Nonetheless, the effectiveness of these different approaches in quantitatively characterizing the distribution of complex canopy APAR remains unknown. Therefore, there is an urgent need to conduct a comparative study on using different crown reconstruction methods derived from ALS to quantify APAR distribution combined with 3D RTMs. This will provide valuable technical methods for acquiring fine-scale light distribution data, thereby enhancing our understanding of ecological processes.

On the other hand, conducting field surveys in complex forests is prone to significant uncertainty due to various environmental factors and measurement errors [27]. Therefore, utilizing a standardized set of forest survey data poses a significant challenge for effectively assessing the ability of different tree crown reconstruction methods to characterize the distribution of complex canopy APAR. Compared to field surveys, utilizing virtual scenes as a benchmark and employing 3D RTMs to simulate radiation transfer information in complex canopies is an alternative option. Currently, the Radiative Transfer Model Intercomparison (RAMI) international RTM community provides various scenes of both real and abstract forest structures to serve as benchmark comparisons between different RTMs [28]. Additionally, to better simulate and understand the capability of LiDAR data signal acquisition for forest structural parameters, some 3D RTMs, such as DART-lux [29] and LESS [30], have also developed LiDAR modules. Therefore, these real RAMI scenes, coupled with the capability of 3D RTMs to simulate LiDAR signals, also provide reliable scene benchmarks and precise structural scanning data for exploring the quantification of APAR distribution using different tree crown reconstruction methods.

In this study, we utilized two real scene structures provided by RAMI as benchmark scene, combined with a 3D RTM LESS to investigate the ability of three crown reconstruction methods (alphashape, ellipsoidal, and voxel-based) to quantify forest canopy APAR distribution. Specifically, we investigated (1) which of the three crown reconstruction approaches is better suited for accurately characterizing the distribution of APAR in complex forest canopies, and (2) the impact of branches on quantifying APAR in the three crown reconstruction methods. The materials and methods are described in Section 2, the results and discussion are presented in Sections 3 and 4, and the conclusions are summarized in Section 5.

2. Material and Methods

2.1. Main Workflow

Utilizing the 3D virtual forest scene provided by fifth phase of radiation transfer model intercomparison (RAMI-V) in conjunction with a 3D RTM, this study evaluates the efficacy of three crown reconstruction methods from ALS point clouds for quantifying APAR. The primary workflow (Figure 1) consists of four components: (1) Typical forest structural scenes from RAMI-V dataset are selected, and ALS point cloud data are simulated using the LiDAR simulation module within a 3D RTM under varied forest structural scenarios including conditions with and without branches. (2) Subsequently, these simulated ALS point cloud data are utilized to reconstruct forest scenes using three crown reconstruction methods (alphashape, ellipsoidal, and voxel-based). (3) Simulation of leaf-scale APAR for the ALS-reconstructed scenes is conducted, along with comparisons to the benchmark RAMI-V scenes. (4) Finally, the APAR characterized by scenes derived from different crown reconstruction methods based on ALS point cloud data is quantitatively

assessed and compared to the APAR characterized in the benchmark RAMI-V scenes. Moreover, the impact of branches on the simulation and quantification of APAR is evaluated in comparison.

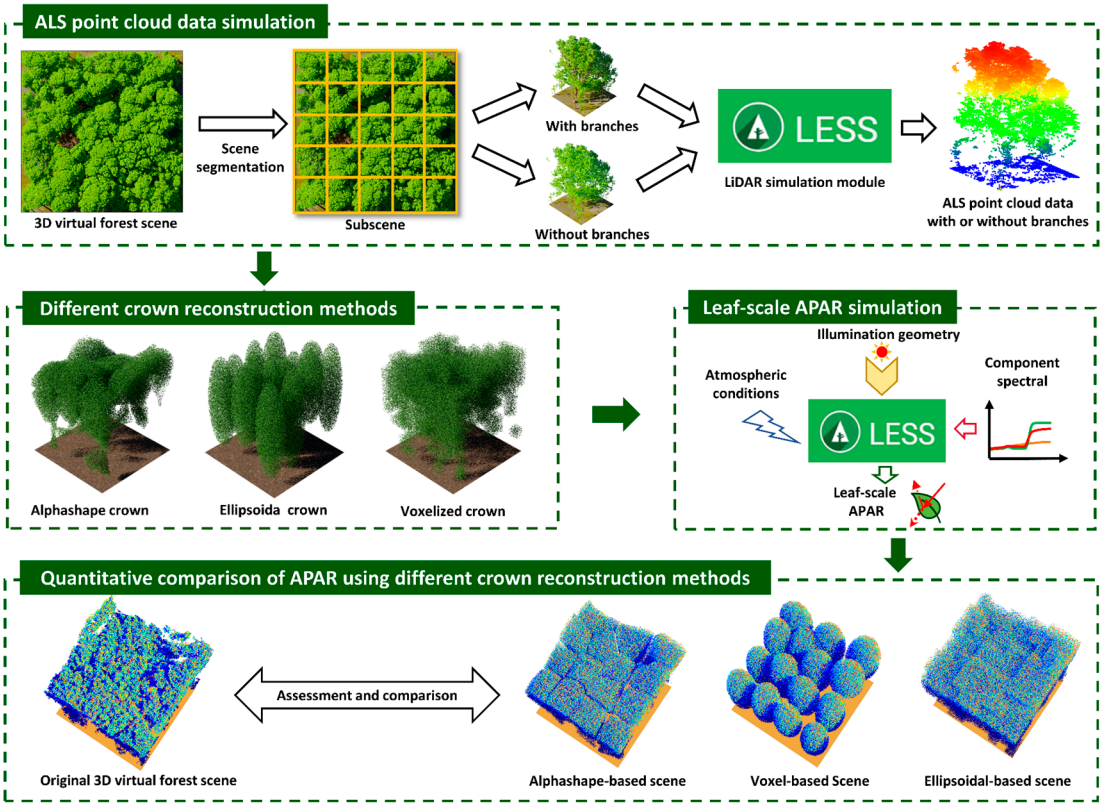


Figure 1. The primary workflow for assessing the capabilities of three crown reconstruction methods in quantifying APAR.

2.2. 3D Virtual Forest Scene

We selected two representative 3D virtual forest scenes from the RAMI-V (Figure 2a,b) dataset to evaluate three crown reconstruction methods for quantifying APAR using a 3D RTM. The first scene, HET09 (Figure 2a), depicts a summer birch forest in Estonia with seven tree species (*Betula pendula*, *Almus glutinosa*, *Acer platanoides*, *Tilia cordata*, *Populus tremuloides*, *Picea abies*, *Fraxinus excelsior*). This scene, created from field measurements taken in the summer of 2017, includes 1029 realistic tree structures, with a leaf area index (LAI) of 3.44, a wood area index (WAI) of 1.92, and a canopy cover fraction of 0.50, covering an area of 105 × 106 m. The second scene, HET51 (Figure 2b), is a one-hectare deciduous broadleaf forest in Wytham, UK, featuring six main tree species (*Acer pseudoplatanus*, *Fraxinus excelsior*, *Quercus robur*, *Corylus avellane*, *Crataegus monogyna*, *Acer campestre*) along with 41 individual trees of unknown species [23]. This scene was reconstructed from terrestrial laser scanning (TLS) data and has a LAI of 3.8, a WAI of 1.92, a canopy cover fraction of 0.90, and dimensions of 100 × 100 m. To facilitate simulations, both scenes were converted into a standard 3D format (e.g., Wavefront OBJ) [31] since the original RAMI-V data could not be directly used in the 3D RTM. Each 3D forest scene was then evenly divided into 25 sub-scenes (Figure 2c,d) to create more detailed structural scenarios for further analysis. This subdivision allowed for a finer examination of light distribution and the performance of different crown reconstruction methods across various canopy structures.

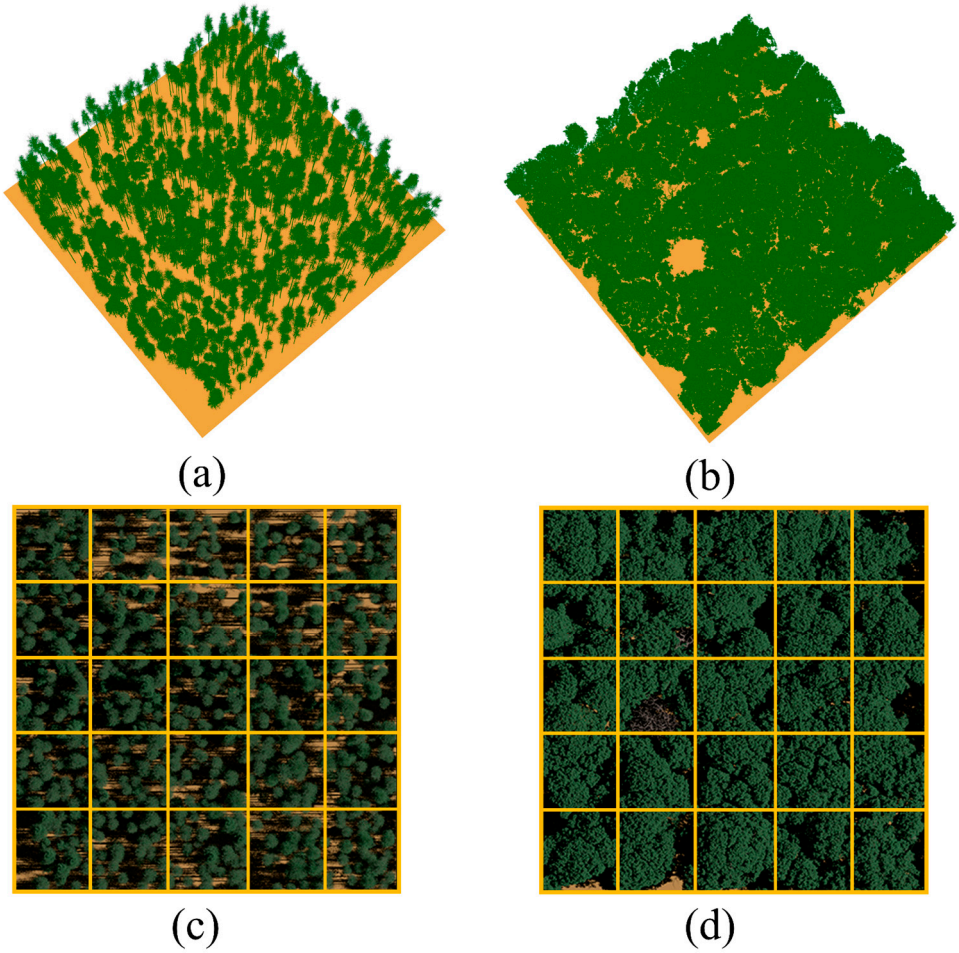


Figure 2. Typical 3D virtual forest scenes provided by RAMI-V. ((**a**,**b**) show the forest scenes HET09 and HET51, respectively. (**c**,**d**) are the RGB orthophotos of these scenes generated using the 3D RTM LESS. Yellow lines indicate the division boundaries for each sub-scene).

2.3. ALS Simulation

The airborne laser scanning (ALS) point cloud data for various virtual forest scenes, as detailed in Section 2.2, were simulated using the LiDAR simulation module of the LESS model [30,32]. LESS (version 2.1.4, http://lessrt.org) is a ray-tracing model that simulates light interactions in realistic scenes, offering both forward and backward ray-tracing modes for various remote sensing signal simulations. This module allows the specification of actual LiDAR device parameters and optical properties of scene elements, enabling the generation of both single-channel and multi-channel point clouds and waveform data. LESS has been extensively applied in previous studies, such as simulating hyperspectral LiDAR point clouds to evaluate the potential of airborne hyperspectral LiDAR for monitoring forest diseases and pests [19], as well as simulation of airborne LiDAR point clouds to validate photon recollision probability (p) estimation algorithms [33]. In this study, we referenced the parameters of a real LiDAR sensor (Riegl VQ-780i, RIEGL Laser Measurement Systems GmbH, Horn, Austria) and configured them (Table 1) within the LiDAR simulation module of LESS to simulate the ALS point cloud data for each virtual forest scene (Figure 3). Specifically, the sensor had a pulse energy of 1 mJ, a laser pulse divergence angle of 0.25 mrad, and an acquisition rate of 0.13 ns, operating at an altitude of 80 m with an across-track and along-track resolution of 0.3 m, resulting in a simulated point density of approximately 10 points/m^2. To further investigate the impact of branches on the APAR using different tree crown reconstruction methods, the branches in each virtual forest

scene were removed. Finally, ALS point cloud data corresponding to forest scenes without branches were also simulated.

Table 1. Riegl VQ-780i LiDAR Sensor Parameter.

Parameters	Values	Unit
Pulse energy	1	mJ
Pulse divergence angle	0.25	mrad
Acquisition rate	0.13	ns
Altitude of flight	80	m
Across-track resolution	0.3	m
Along-track resolution	0.3	m

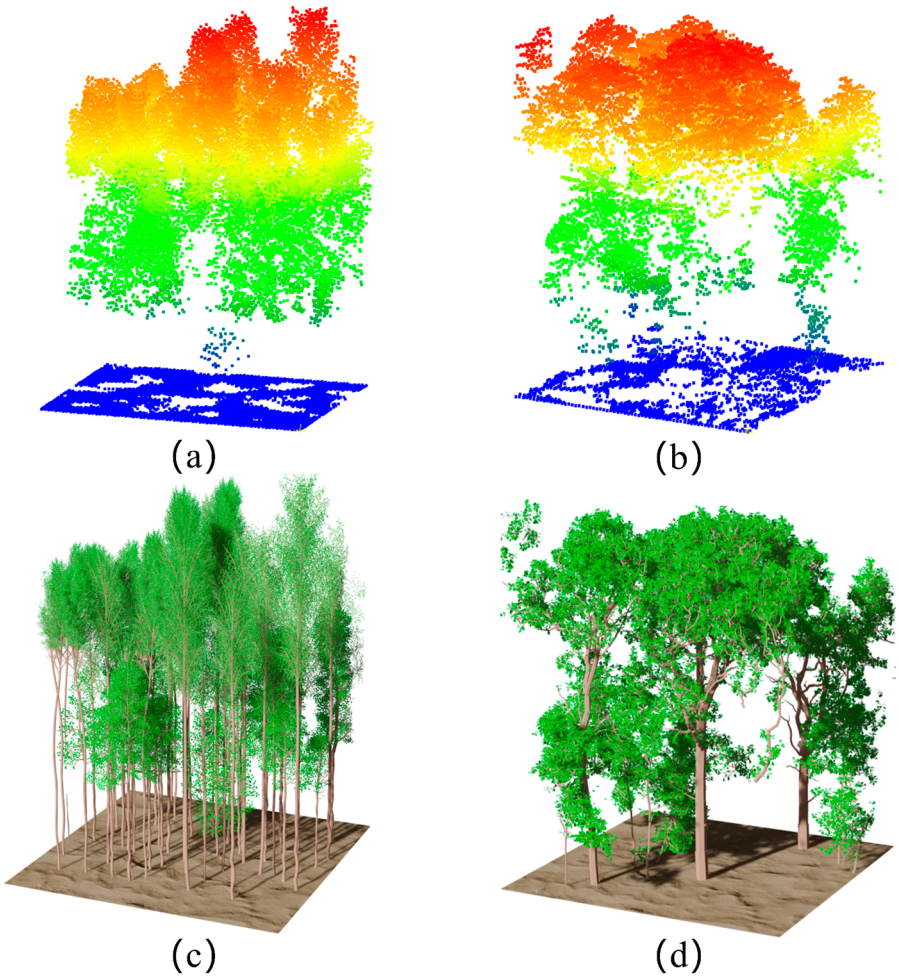


Figure 3. Virtual forest scene ALS (airborne laser scanning) point cloud data simulated using the LESS LiDAR module. (Sub-scenes (**c**) from HET09 and Sub-scenes (**d**) from HET51 are represented as point clouds (**a**,**b**), respectively).

2.4. Crown Reconstruction from ALS

To evaluate and compare the capabilities of the three tree crown reconstruction methods for quantifying leaf-scale APAR, we employed alphashape, voxel, and ellipsoid-based methods to reconstruct 3D virtual forest scenes from the ALS data described in Section 2.3. In the alphashape-based crown reconstruction method, a cloth simulation filter (CSF) [34] algorithm classifies ALS data into ground and vegetation points. A combination of watershed segmentation and k-means clustering algorithm [13] is then used to group vegetation points into clusters. Each cluster is processed with the alphashape algorithm [35] to create a geometric envelope for the sub-crown, while the ground points are rasterized into a digital

elevation model (DEM) to represent the actual terrain. Subsequently, voxel-based and ellipsoid-based methods are also implemented. For terrain reconstruction, the methods using the voxel-based and ellipsoid-based methods are the same as the alphashape-based crown reconstruction method. For the voxel-based crown reconstruction method, we set a voxel resolution of 1 m to uniformly enclose each vegetation point cloud cluster within small cubes. For spatial positions without point cloud distribution, no voxels are created. This allows us to account for computational efficiency while also achieving a detailed reconstruction of the voxel-based crown. Previous studies have demonstrated that scenes reconstructed with a 1 m voxel resolution can effectively simulate canopy reflectance information [36]. In the ellipsoid-based crown reconstruction method, we use each vegetation point cloud cluster and calculate their spatial dimensions of length and width. Subsequently, each ellipsoid crown envelope is directly fitted based on the calculated dimensions of each point cloud cluster. After completing the reconstruction of different crown scenarios, we use a plant area density (PAD) estimation method [37] derived from ALS data to parameterize each sub-crown. Specifically, based on the estimated PAD values, square faces with an area of 0.01 m^2 serve as leaves [38], filling each sub-crown to facilitate the simulation of leaf-scale APAR. The PAD within each sub-crown can be calculated using the Beer–Lambert Law as follows:

$$\mathrm{PAD} = \frac{\sum_1^n \left(-\frac{\ln T_j}{G(\Omega)\Delta l_j} \right)}{n} - \quad (1)$$

where n denotes the number of pulses transmitted through each tree crown, and $G(\Omega)$ represents the projection coefficient of crown foliage in the Ω direction. In this study, we assume a leaf inclination angle distribution within the crown that follows a spherical distribution. Therefore, $G(\Omega) = 0.5$. Δl_j is the path length for pulse j as it traverses each tree crown (i.e., alphashape, ellipsoid, and voxel). T_j is the transmittance of pulse j through the corresponding tree crown. Furthermore, the transmittance T_j can be calculated based on the ratio of the outgoing energy I_j^{out} to the incoming energy I_j^{in}, which is derived from the intensity of the ALS point cloud data. The incident energy I_j^{in} is determined at the location of each LiDAR return. The outgoing energy I_j^{out}, in turn, represents the incident energy of subsequent volumes within the tree crown, which can be iteratively calculated in the same manner as the incident energy.

2.5. Leaf-Scale APAR Simulation

We utilized reconstructed forest scenes, as detailed in Section 2.4, to simulate leaf-scale APAR using LESS [14]. We employed the forward ray-tracing mode to simulate leaf-scale APAR, accounting for the physical interactions between photons and scene elements at each collision point. By explicitly considering the optical properties of each element, we enabled precise calculations of light absorption and scattering. Furthermore, APAR energy can be accumulated at various levels, including individual leaves, canopy vertical stratification, or specific tree elements (e.g., leaves, branches). The detailed calculation process of APAR in the LESS model has also been found in previous studies [14]. In fact, LESS has been used in past research to simulate daily-scale tree APAR for quantitative analysis of the relationship between light and tree structure [9]. It has also been applied to simulate the absorption of photosynthetically active radiation by green vegetation, aiding in the validation of FAPAR inversion algorithms [39].

In this study, we parameterized the LESS model based on the research of Zhao et al., 2024 [9], simulating absorbed photosynthetically active radiation (APAR) across a spectral range of 400–700 nm with a spectral resolution of 1 nm. We initially defined a spectral curve measured using a ground-based ASD spectrometer (FieldSpec4 Hi-Res NG) for leaves,

branches, and soil. This ensured minimal interference from variations in optical properties, allowing a more focused analysis of the impact of canopy structure on APAR. To account for atmospheric effects, we integrated the 6S atmospheric model [40] to calculate sky scattering and direct solar radiation at noon for each virtual forest scene reconstructed using different methods from ALS. Finally, we used the LESS model to complete the leaf-scale APAR simulation for each forest scene at noon. For comparison, the leaf-scale APAR for each sub-scene from the two benchmark scenarios, HET09 and HET51, were also simulated.

2.6. Assessment and Comparison

We used sub-scenes from the HET09 and HET51 scenarios as benchmarks to evaluate various tree crown reconstruction methods for quantifying APAR. To analyze APAR's vertical distribution, we stratified the APAR values at 1 m height intervals for each sub-scene. Within each stratum, we summed the leaf-scale APAR values to determine cumulative APAR, creating a detailed vertical profile of the forest canopy. We also calculated the Leaf Area Index (LAI) at 1 m intervals using the 3D LAI calculator from the LESS model for comparison. Furthermore, three assessment metrics (the root mean square error (RMSE), mean absolute error (MAE), and mean absolute percentage error (MAPE)) were also used to quantitatively evaluate the impact of different tree crown reconstruction methods and the branches on APAR simulation.

3. Results

3.1. Visualization Comparison of 3D APAR Distribution

Two typical forest sub-scenes, A and B (Figure 4), with distinct crown structure distributions were selected from HET09 and HET51 to visually assess and compare the capabilities of various crown reconstruction methods in characterizing 3D APAR. These forest sub-scenes, along with the benchmark ones, were rendered from a nadir perspective using Blender software (version 3.1). It can be observed from Figure 4 that the typical sub-scene A selected from HET09 is relatively sparse and discontinuous, with a canopy coverage of 0.4 (Figure 4a), whereas the typical sub-scene B selected from HET51 is a dense and continuous, with a canopy coverage of 0.9 (Figure 4e). Furthermore, the 3D APAR distributions and local visualizations of these scenes are presented in Figure 5. To facilitate visual comparison at the leaf scale, the simulated APAR energy for each sub-scene is also converted into APAR per unit area. Overall, it can be seen from Figure 5 that more light is intercepted by the top of the forest canopy. Among the methods, the alphashape-based approach maintains more gaps between crowns, while the ellipsoid-based method creates crowns with a more independent distribution, allowing greater light penetration to middle or lower canopy layers. In contrast, the voxel-based method misses smaller gaps, resulting in reduced light reaching the middle or lower parts of the canopy compared to the other two methods.

3.2. Comparison of APAR in the Vertical Profile of Canopy

The 3D APAR profile distributions of sub-scenes, A and B (Figure 4), selected from the HET09 and HET51 scenarios are presented in Figures 6 and 7, respectively. It can be observed from Figures 6 and 7 that for both sub-scenes, regardless of whether they are benchmark scenes or ALS-reconstructed scenes using three crown reconstruction methods, the 3D APAR exhibits an increasing and then decreasing trend from the bottom to the top of the canopy. Among the 3D APAR profile curves of the ALS-reconstructed scenes using the three crown reconstruction methods, the alphashape-based crown reconstruction method is more consistent with that of the benchmark scenes, compared to those reconstructed using the ellipsoid and voxel methods. Similarly, the LAI vertical profile distribution curve

of the scenes reconstructed using the alphashape-based crown reconstruction method is also more consistent with that of the benchmark scenes, compared to those reconstructed using the ellipsoid and voxel methods.

3.3. Quantitative Comparison of 3D APAR

In order to quantitatively compare and evaluate the ability of different tree crown reconstruction methods to depict the APAR in 3D forest scenes with and without branches, we calculated the total APAR value for each scene by summing the leaf-scale APAR. Figure 8 presents scatter plots comparing APAR across different reconstruction methods and the benchmark scenes for HET09 (Figure 8a,b) and HET51 (Figure 8c,d), including both branched (Figure 8a,c) and branchless (Figure 8b,d) conditions. It can be observed from Figure 8 that, for the ALS-reconstructed scenes, the deviation between the APAR characterized by the alphashape-based crown reconstruction and the benchmark scene APAR is the smallest, followed by the ellipsoid-based reconstruction, while the voxel-based reconstruction method shows the largest deviation. To further compare the differences among tree crown reconstruction methods in characterizing APAR under both branched and branchless conditions (Figure 9), we calculated the RMSE (Figure 9a,d), MAE (Figure 9b,e), and MAPE (Figure 9c,f) metrics for each crown reconstruction method. These statistical assessment metrics, along with those for the benchmark scene, were calculated and presented as bar charts for the HET09 and HET51 scenes. It can be observed from Figure 9 that under both branched and branchless conditions, the overall differences in APAR characterization among the three crown reconstruction methods are minimal compared to the benchmark scene. The largest RMSE differences are 3.67 kW, the largest MAE differences are 1.49 kW, and the MAPE for all three crown reconstruction methods remains below 1.16%.

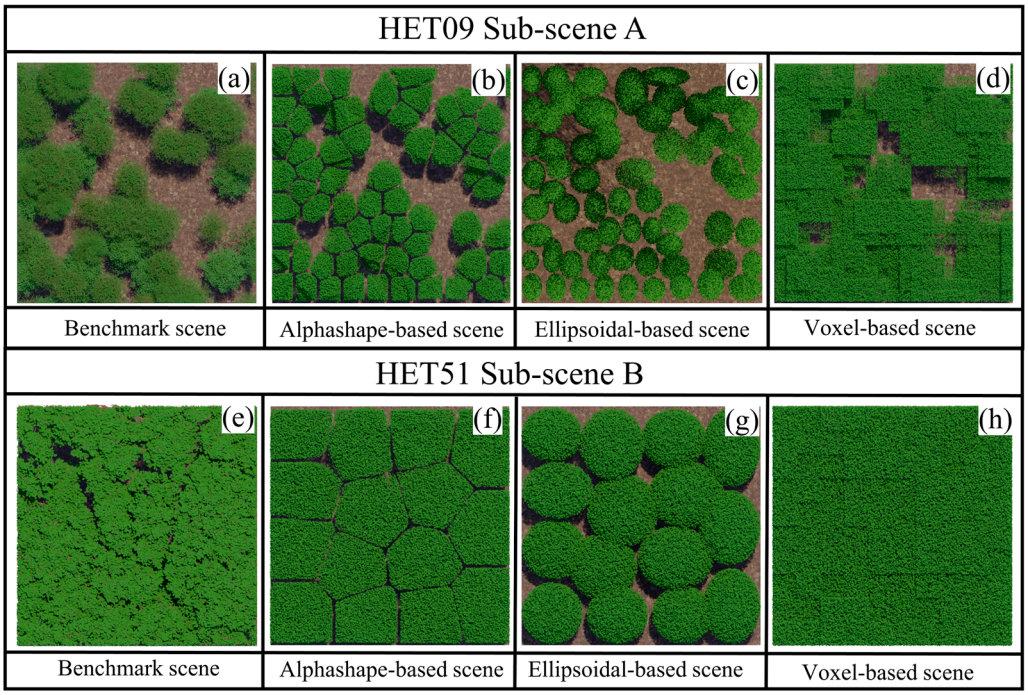


Figure 4. Two typical forest sub-scenes, A and B, selected from HET09 (**a**) and HET51 (**e**), respectively, along with their corresponding scenes generated using different crown reconstruction methods, are shown from a nadir perspective rendered with Blender software. Panels (**b**–**d**) illustrate the tree crowns reconstructed using the alphashape-based method, ellipsoid-based method, and voxel-based method for HET09 Sub-scene A. Similarly, panels (**f**–**h**) show the tree crowns reconstructed using the same methods for HET51 Sub-scene B.

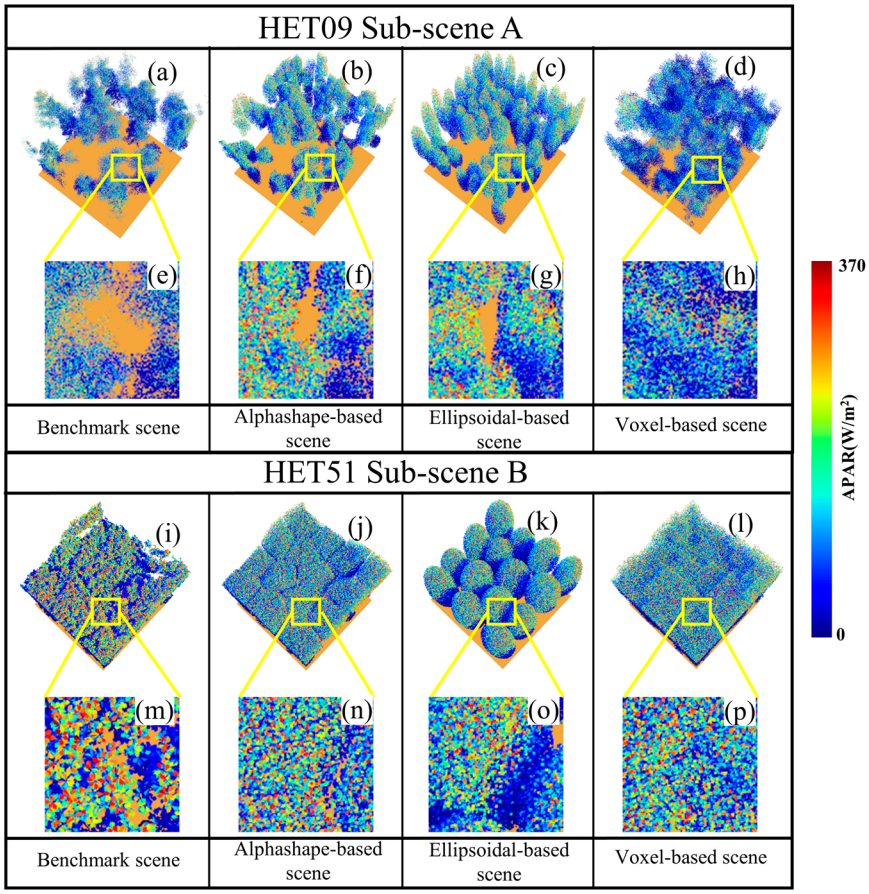


Figure 5. 3D APAR distribution of two typical sub-scenes, A and B (Figure 4), selected from HET09 (**a**) and HET51 (**i**), with their corresponding local views shown in (**e**,**m**), respectively. The 3D APAR distributions of the scenes generated using different crown reconstruction methods are also presented. For HET09 Sub-scene A, panels (**b**–**d**,**f**–**h**) display the panoramic and local views, respectively, for the alphashape-based, ellipsoid-based, and voxel-based methods. Similarly, for HET51 Sub-scene B, panels (**j**–**l**,**n**–**p**) show the panoramic and local views for the same methods.

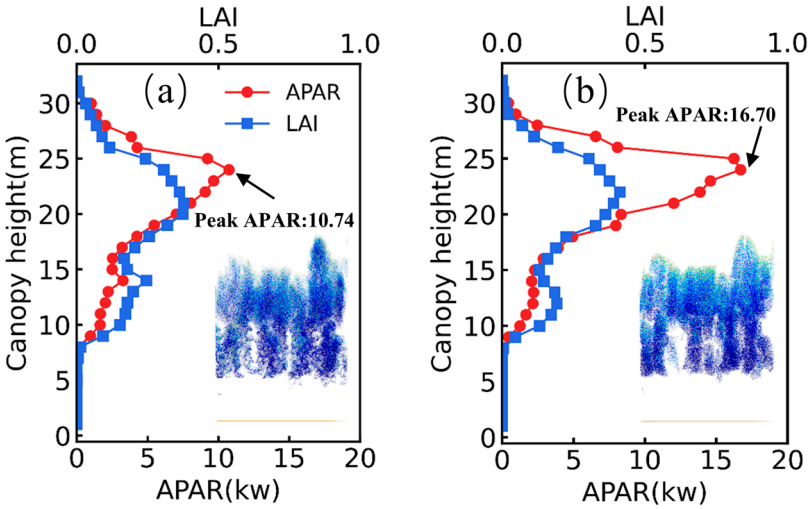


Figure 6. *Cont.*

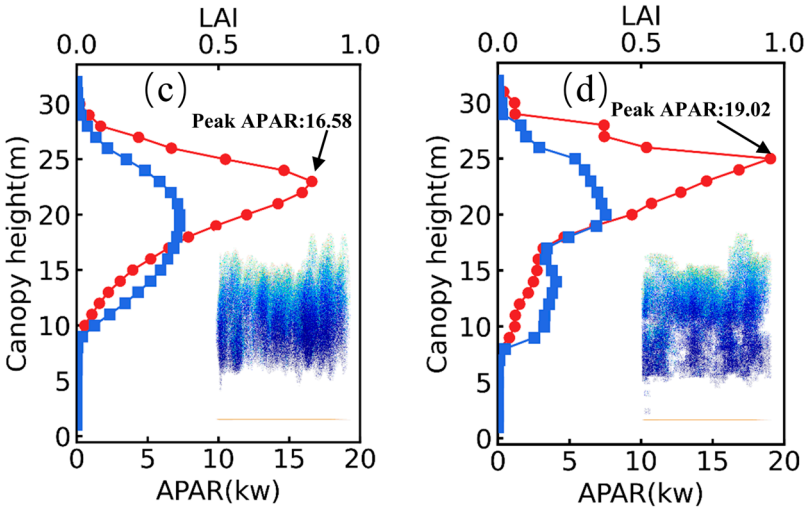


Figure 6. HET09 sub-scene A canopy vertical profile APAR distribution ((**a**) represents the benchmark scene, while (**b**–**d**) depict scenes reconstructed using the alphashape, ellipsoid, and voxel-based crown reconstruction methods, respectively).

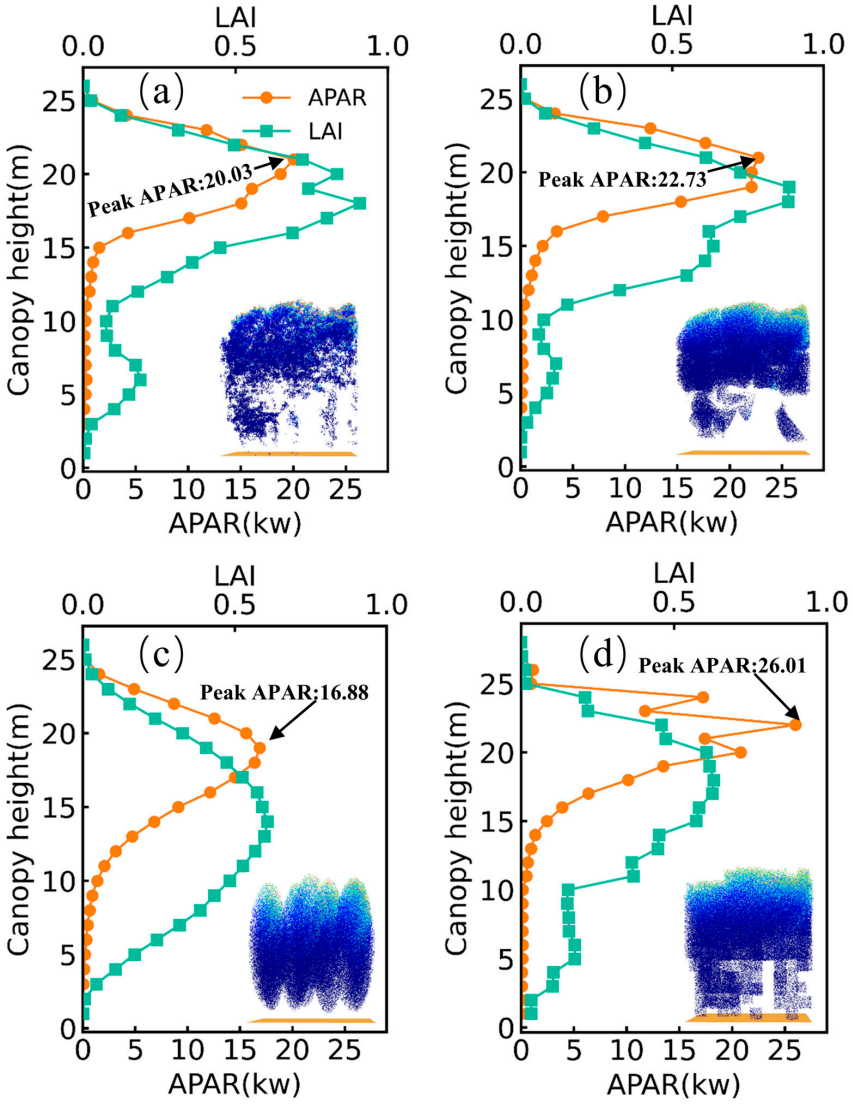


Figure 7. HET51 sub-scene B canopy vertical profile APAR distribution ((**a**) represents the benchmark scene, while (**b**–**d**) depict scenes reconstructed using the alphashape, ellipsoid, and voxel-based crown reconstruction methods, respectively).

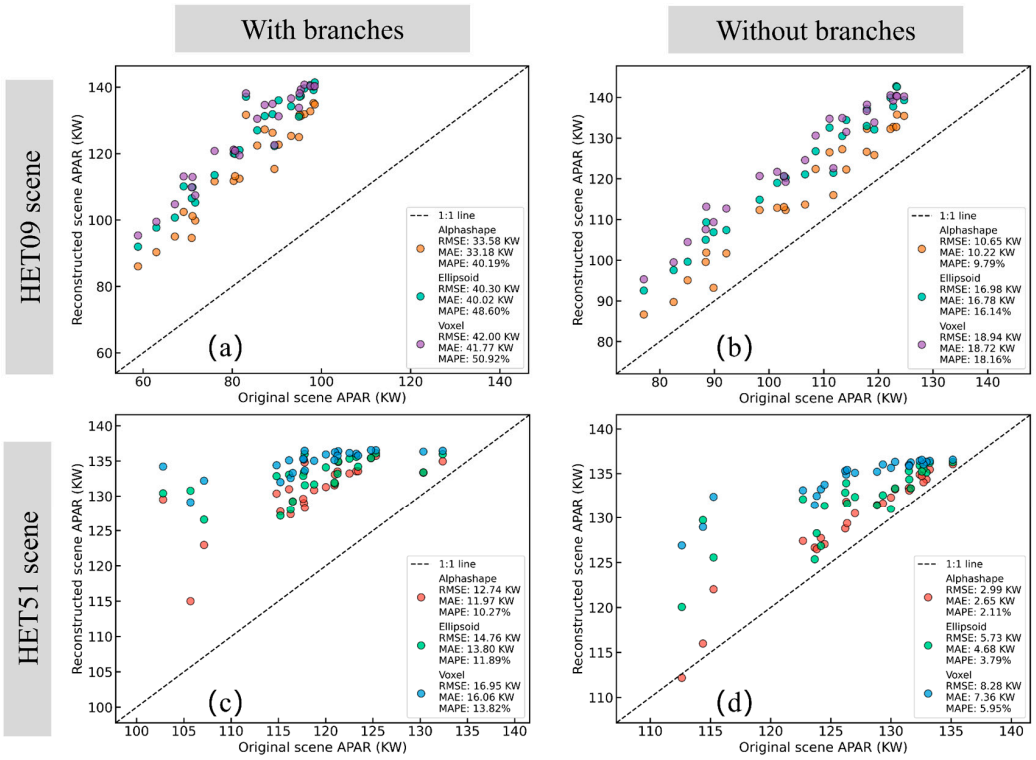


Figure 8. Comparison of the ability to characterize APAR between ALS-reconstructed scenes and the benchmark scene (**a**,**b**) show comparisons for the HET09 under branched and branchless conditions, respectively; (**c**,**d**) show comparisons for the HET51 under branched and branchless conditions, respectively.

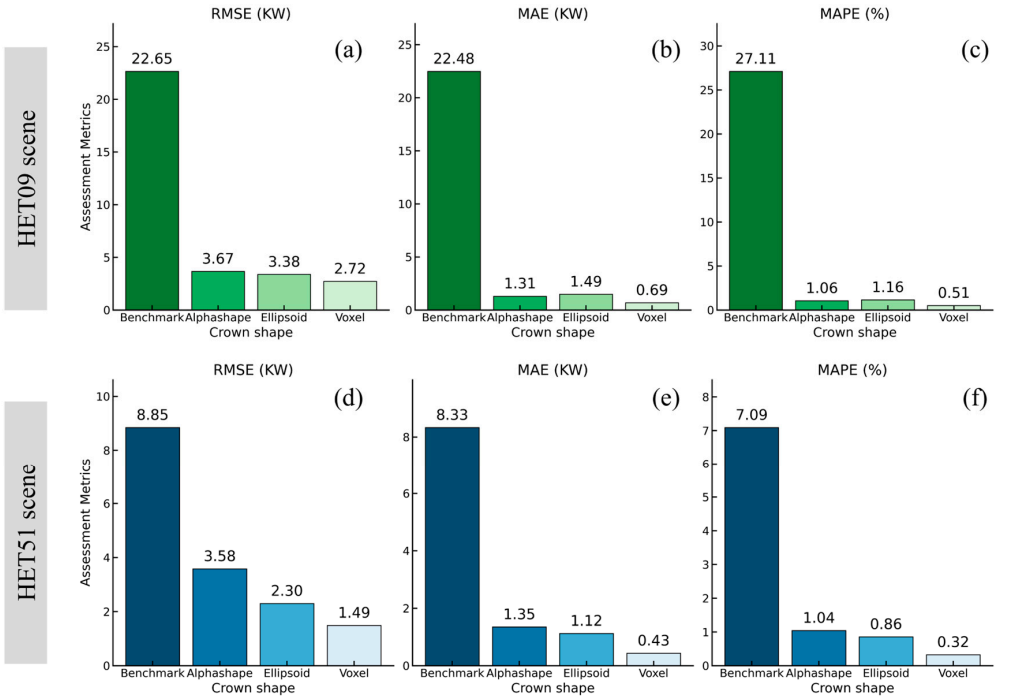


Figure 9. Comparison of APAR characterization using the benchmark scene and three crown reconstruction methods (alphashape, ellipsoid, voxel-based) under both branched and branchless conditions (**a**–**c**) present the RMSE, MAE, and MAPE assessment metrics for the HET09 scene, while (**d**–**f**) present the RMSE, MAE, and MAPE metrics for the HET51 scene.

4. Discussion

4.1. Impact of Crown Reconstruction Methods on APAR Simulation

In this study, we utilized three crown reconstruction methods (alphashape, ellipsoid, and voxel-based) based on ALS point cloud data to complete the reconstruction of forest scenes. Subsequently, an advanced 3D radiative transfer model, LESS, was employed to simulate leaf-scale APAR (absorbed photosynthetically active radiation) for both the ALS-reconstructed forest scenes and the corresponding benchmark scenes. The three crown reconstruction methods exhibit varying degrees of geometric variation in crown shapes (Figure 4). Previous studies have shown that differences in crown shapes structure influence canopy interception and result in variations in light distribution within the vegetation canopy [41,42]. Furthermore, in both the HET09 sub-scene A sparse (Figure 6) and HET51 sub-scene B dense (Figure 7) forest scenes, through the visualization of the 3D APAR distribution for the three crown reconstruction methods (Figure 5), the comparison of their APAR distribution in vertical canopy profiles (Figures 6 and 7), and a quantitative comparison with the benchmark scenes (Figure 8). Our findings indicate that the alpha-shape-based crown reconstruction method offers a more accurate quantification of canopy APAR distribution, aligning closely with the benchmark scenes APAR distribution. This result is primarily attributed to the alphashape-based crown reconstruction method's ability to better fit the geometric shape of the tree crown during reconstruction, preserving the subtle gaps between the crown edges, thus more accurately representing the actual boundary of the tree crown. Compared to ellipsoid and voxel-based methods, previous studies have also shown that the canopy reflectance simulated by the alphashape-based crown reconstruction method is more aligned with benchmark forest scenes [13], which is consistent with our quantitative APAR comparison results for different tree crown reconstruction methods. Moreover, the ellipsoid-based tree crown reconstruction method encounters difficulties in depicting leaf-scale APAR, as it struggles to accurately capture the complex structure of the forest canopy due to the relatively independent nature of the ellipsoid-shaped crowns (Figure 4c,g). This results in a smoother light distribution in the vertical profile of the forest, particularly at the top of the canopy, where the discrepancy in light distribution compared to the benchmark scene is greatest. For the voxel-based method, small gaps between tree crowns are often overlooked during the reconstruction process (Figure 4d,h), resulting in the upper canopy intercepting the most of the light. Consequently, compared to the alphashape and ellipsoid-based crown reconstruction methods, the peak values of APAR in the vertical profile of the canopy are highest in voxel-based reconstructed scenes for both the HET09 sub-scene A (Figure 6d) and HET51 sub-scene B (Figure 7d) scenes. Additionally, this method tends to fill these small gaps within the tree crown [25], leading to discrepancies in light distribution in the vertical canopy profile compared to the benchmark scene.

In the process of scene reconstruction, although the plant area density (PAD) estimated using ALS point cloud data ensure the accuracy of the canopy structure, the random distribution of leaves within the crown makes it difficult to maintain the benchmark arrangement of leaves. This results in a reduction in the clumping effect among the leaves. Compared with the benchmark forest scene, this distribution makes it more likely for leaves within the canopy to intercept direct radiation and scattered light from surrounding leaves. Consequently, we observe that the simulated scenes from the three crown reconstruction methods generally exhibit a trend of higher absorbed photosynthetically active radiation (APAR) compared to the benchmark scene (Figure 8).

In addition to the impact of tree crown geometry and leaf spatial distribution on the differences in light distribution between reconstructed 3D forest scenes and benchmark forest scenes, the leaf angle distribution is also an important factor affecting the light distri-

bution within the forest canopy [7]. In this study, we used a spherical distribution function to describe the leaf angle distribution in three crown reconstruction methods, which is another factor contributing to the discrepancies in the 3D APAR distribution between the different tree crown reconstruction methods and the benchmark scenes. Therefore, accurate measurements of leaf angles are crucial for using airborne LiDAR to reconstruct forest scenes and quantify light distribution. However, it is important to acknowledge that measuring leaf angles in natural forests presents a significant challenge. Previous studies have shown that employing high-resolution ground-based LiDAR for precise leaf angle measurements is a promising approach [43].

4.2. Impact of Branches

In this study, while the reconstructed scenes using the three crown reconstruction methods from ALS provided a detailed foundation for quantifying light distribution within forests, we found that branches play a crucial role in accurately representing the forest's 3D APAR distribution. It can be seen from Figure 8 that for both the HET09 and HET51 scenes, the APAR characterized by ALS-reconstructed forest scenes shows that the evaluation metrics (RMSE, MAE, MAPE) for the scenes before branch removal (Figure 8a,c) are significantly higher than those for the scenes after branch removal (Figure 8b,d), compared to the benchmark scene. This discrepancy primarily arises from the reconstruction process of forest scenes using ALS point clouds, where branch and leaf point clouds are not distinguished. We used all crown point clouds to estimate the plant area density (PAD) and serve as reference values for filling the crown envelope with leaves. In contrast, in the benchmark scenes, branches and leaves are distinct components, resulting in the ALS-reconstructed forest scenes intercepting more light compared to the benchmark scenes. Furthermore, we compared the impact of different tree crown reconstruction methods on the quantification of APAR distribution before and after branch removal (Figure 9). Compared to ellipsoid and voxel-based crown reconstruction methods, the differences in quantified APAR before and after branch removal are more consistent with those of the benchmark scenes when using the alphashape-based crown reconstruction method. It is worth noting that the impact of using ALS to reconstruct forest scenes with branches on the quantification of APAR varies across different forest structures. In the case of HET09, which features a sparse canopy with a relatively low canopy cover (0.5), more laser pulses capture branch point cloud data during forest scanning. As a result, the influence of branches on APAR quantification is more significant for HET09, regardless of the crown reconstruction methods. In contrast, for HET51, which has a dense and continuous canopy distribution with a high canopy cover of 0.9, the majority of the point cloud is intercepted by upper vegetation leaves, resulting in fewer branch point clouds. Consequently, the difference in APAR quantification before and after removing branches in the HET51 scene is minimal, consistent with the results from the benchmark scene before and after branch removal.

4.3. Limitations

In this study, we utilized a 3D radiative transfer model in conjunction with ALS-reconstructed forest scenes to assess the capabilities of various tree crown reconstruction methods in characterizing the 3D distribution of APAR within forest canopies. The high-resolution forest structural data provided by advanced LiDAR technology laid a solid foundation for reconstructing 3D virtual forest scenes. Moreover, the state-of-the-art 3D radiative transfer model LESS offered a convenient technical tool for quantifying and simulating the radiative information of forest canopies. However, when employing the voxel-based crown reconstruction method, the impact of different voxel resolutions on the quantification of 3D APAR requires further investigation. Additionally, while we calibrated

leaf areas using PAD estimates derived from LiDAR point clouds, the reconstruction of leaf models that account for actual leaf shapes and dimensions merits further exploration. Furthermore, the separation of branch and leaf point clouds from LiDAR data to create forest scenes with distinct structural elements (e.g., branches and leaves) [44,45] presents a promising approach for accurately quantifying APAR at a regional scale. Finally, for our study, we primarily used two virtual forest scenes to investigate different tree crown reconstruction methods for quantifying APAR. While subdividing these scenes into sub-scenes allowed us to capture a more diverse range of forest structures (e.g., different densities and coverages), a broader range of forest types should be tested in future work. Besides these, the impact of different environmental factors, such as terrain, altitude, and the spatiotemporal variation of APAR at daily and seasonal scales, also deserves further exploration.

5. Conclusions

In this study, we first selected two structurally explicit 3D virtual forest scenes from the RAMI-V as benchmark reference scenarios. These scenes were integrated with the 3D radiative transfer model LESS to simulate ALS point cloud data. We then reconstructed the forest scenes from these simulated ALS point clouds using three tree crown reconstruction methods to assess their effectiveness in quantifying the 3D distribution of APAR within forest canopies with the LESS model. For comparison, we quantitatively simulated the APAR of the benchmark scenarios using the LESS model. Moreover, we investigated the impact of branches on various tree crown reconstruction methods for quantifying APAR. In the forest scenarios of HET09 and HET51, which represent different crown distribution types, both visual and quantitative assessments indicate that the alphashape-based crown reconstruction method more closely approximates the 3D APAR distribution of the benchmark scenes than do ellipsoid and voxel-based crown reconstruction methods. Furthermore, the vertical APAR profile curves depicted by the alphashape-based method also align more consistently with the vertical APAR curves of the benchmark scenes. In the quantitative comparison of APAR, the alphashape-based crown reconstruction method exhibited the smallest differences in assessment metrics compared to the benchmark scenes, as opposed to ellipsoid and voxel-based methods. Specifically, for the scenarios with and without branches, the assessment metrics for HET09 are as follows: RMSE 33.58 kW, MAE 33.18 kW, and MAPE 40.19% (after branch removal: RMSE 10.65 kW, MAE 10.22 kW, MAPE 9.79%). The corresponding metrics for HET51 are as follows: RMSE 12.74 kW, MAE 12.97 kW, and MAPE 10.27% (after branch removal: RMSE 2.99 kW, MAE 2.65 kW, MAPE 2.11%). Furthermore, compared to ellipsoid and voxel-based methods, the alphashape-based method showed the largest differences in RMSE, MAE, and MAPE between scenarios with and without branches. However, when compared to the APAR assessment metrics of the benchmark scenes before and after branch removal, the alphashape-based method's assessment metrics RMSE, MAE, and MAPE are closer to those of the benchmark reference scenes. The conclusion demonstrates that integrating ALS point cloud data with the alphashape-based crown reconstruction method can potentially offer strong support for simulating and quantifying forest APAR on a large scale. This approach enables the acquisition of fine-scale light distribution data, which can serve as a foundation for understanding ecologically relevant processes such as photosynthesis and forest growth dynamics. However, when using ALS point clouds and the 3D RTMs for the quantitative simulation of APAR distribution, the impact of branches is a critical factor that should not be overlooked.

Author Contributions: Conceptualization, X.Z.; Methodology, X.Z.; Software, X.Z., L.Y. and Z.Y.; Formal analysis, C.L., J.Q. and L.Y.; Data curation, L.Y.; Writing—original draft, X.Z.; Writing—review & editing, X.Z., C.L., J.Q., Z.Y., S.H. and H.H.; Visualization, X.Z.; Supervision, C.L., J.Q. and H.H. All authors have read and agreed to the published version of the manuscript.

Funding: This work was supported by the National Natural Science Foundation of China (Grant No. 42371345, Grant No. 42192580),the Beijing Nova Program (20240484556) and the Fundamental Research Funds for the Central University.

Data Availability Statement: The scene data used in this study are publicly available and can be accessed via the following link: http://lessrt.org/resources/3dscene/.

Conflicts of Interest: The authors declare no conflicts of interest.

References

1. Liu, R.; Ren, H.; Liu, S.; Liu, Q.; Li, X. Modelling of Fraction of Absorbed Photosynthetically Active Radiation in Vegetation Canopy and Its Validation. *Biosyst. Eng.* **2015**, *133*, 81–94. [CrossRef]
2. Hilker, T.; Coops, N.C.; Wulder, M.A.; Black, T.A.; Guy, R.D. The Use of Remote Sensing in Light Use Efficiency Based Models of Gross Primary Production: A Review of Current Status and Future Requirements. *Sci. Total Environ.* **2008**, *404*, 411–423. [CrossRef] [PubMed]
3. Kesselring, J.; Morsdorf, F.; Kükenbrink, D.; Gastellu-Etchegorry, J.-P.; Damm, A. Diversity of 3D APAR and LAI Dynamics in Broadleaf and Coniferous Forests: Implications for the Interpretation of Remote Sensing-Based Products. *Remote Sens. Environ.* **2024**, *306*, 114116. [CrossRef]
4. Ma, H.; Liu, Q.; Liang, S.; Xiao, Z. Simultaneous estimation of leaf area index, fraction of absorbed photosynthetically active radiation, and surface albedo from multiple-satellite data. *IEEE Trans. Geosci. Remote Sens.* **2017**, *55*, 4334–4354. [CrossRef]
5. Pei, Y.; Dong, J.; Zhang, Y.; Yuan, W.; Doughty, R.; Yang, J.; Zhou, D.; Zhang, L.; Xiao, X. Evolution of Light Use Efficiency Models: Improvement, Uncertainties, and Implications. *Agric. For. Meteorol.* **2022**, *317*, 108905. [CrossRef]
6. Senna, M.C.A.; Costa, M.H.; Shimabukuro, Y.E. Fraction of Photosynthetically Active Radiation Absorbed by Amazon Tropical Forest: A Comparison of Field Measurements, Modeling, and Remote Sensing. *J. Geophys. Res. Biogeosci.* **2005**, *110*, G01008. [CrossRef]
7. Kükenbrink, D.; Schneider, F.D.; Schmid, B.; Gastellu-Etchegorry, J.-P.; Schaepman, M.E.; Morsdorf, F. Modelling of Three-Dimensional, Diurnal Light Extinction in Two Contrasting Forests. *Agric. For. Meteorol.* **2021**, *296*, 108230. [CrossRef]
8. Xue, X.; Jin, S.; An, F.; Zhang, H.; Fan, J.; Eichhorn, M.P.; Jin, C.; Chen, B.; Jiang, L.; Yun, T. Shortwave Radiation Calculation for Forest Plots Using Airborne LiDAR Data and Computer Graphics. *Plant Phenomics* **2022**, *2022*, 9856739. [CrossRef]
9. Zhao, X.; Qi, J.; Yu, Z.; Yuan, L.; Huang, H. Fine-Scale Quantification of Absorbed Photosynthetically Active Radiation (APAR) in Plantation Forests with 3D Radiative Transfer Modeling and LiDAR Data. *Plant Phenomics* **2024**, *6*, 166. [CrossRef]
10. Sitch, S.; Smith, B.; Prentice, I.C.; Arneth, A.; Bondeau, A.; Cramer, W.; Kaplan, J.O.; Levis, S.; Lucht, W.; Sykes, M.T.; et al. Evaluation of Ecosystem Dynamics, Plant Geography and Terrestrial Carbon Cycling in the LPJ Dynamic Global Vegetation Model. *Glob. Change Biol.* **2003**, *9*, 161–185. [CrossRef]
11. Scott Denning, A.; Nicholls, M.; Prihodko, L.; Baker, I.; Vidale, P.-L.; Davis, K.; Bakwin, P. Simulated Variations in Atmospheric CO_2 over a Wisconsin Forest Using a Coupled Ecosystem–Atmosphere Model. *Glob. Change Biol.* **2003**, *9*, 1241–1250. [CrossRef]
12. Gastellu-Etchegorry, J.-P.; Yin, T.; Lauret, N.; Cajgfinger, T.; Gregoire, T.; Grau, E.; Feret, J.-B.; Lopes, M.; Guilleux, J.; Dedieu, G.; et al. Discrete Anisotropic Radiative Transfer (DART 5) for Modeling Airborne and Satellite Spectroradiometer and LIDAR Acquisitions of Natural and Urban Landscapes. *Remote Sens.* **2015**, *7*, 1667–1701. [CrossRef]
13. Qi, J.; Xie, D.; Jiang, J.; Huang, H. 3D Radiative Transfer Modeling of Structurally Complex Forest Canopies through a Lightweight Boundary-Based Description of Leaf Clusters. *Remote Sens. Environ.* **2022**, *283*, 113301. [CrossRef]
14. Qi, J.; Xie, D.; Yin, T.; Yan, G.; Gastellu-Etchegorry, J.-P.; Li, L.; Zhang, W.; Mu, X.; Norford, L.K. LESS: LargE-Scale Remote Sensing Data and Image Simulation Framework over Heterogeneous 3D Scenes. *Remote Sens. Environ.* **2019**, *221*, 695–706. [CrossRef]
15. Bian, Z.; Wu, S.; Roujean, J.-L.; Cao, B.; Li, H.; Yin, G.; Du, Y.; Xiao, Q.; Liu, Q. A TIR Forest Reflectance and Transmittance (FRT) Model for Directional Temperatures with Structural and Thermal Stratification. *Remote Sens. Environ.* **2022**, *268*, 112749. [CrossRef]
16. Gao, S.; Zhong, R.; Yan, K.; Ma, X.; Chen, X.; Pu, J.; Gao, S.; Qi, J.; Yin, G.; Myneni, R.B. Evaluating the Saturation Effect of Vegetation Indices in Forests Using 3D Radiative Transfer Simulations and Satellite Observations. *Remote Sens. Environ.* **2023**, *295*, 113665. [CrossRef]
17. Makhloufi, A.; Kallel, A. Inversion of a New Designed ANN-Based 3-D-RTM Emulator by Continuous MCMC Technique to Monitor Crop Biophysical Properties Using Sentinel-2 Images. *IEEE Trans. Geosci. Remote Sens.* **2023**, *61*, 1–14. [CrossRef]

18. Lin, S.; Li, L.; Liu, S.; Gao, G.; Zhao, X.; Chen, L.; Qi, J.; Shen, Q.; Huang, H. Stratified Burn Severity Assessment by Integrating Spaceborne Spectral and Waveform Attributes in Great Xing'an Mountain. *Remote Sens. Environ.* **2024**, *307*, 114152. [CrossRef]
19. Zhao, X.; Qi, J.; Xu, H.; Yu, Z.; Yuan, L.; Chen, Y.; Huang, H. Evaluating the Potential of Airborne Hyperspectral LiDAR for Assessing Forest Insects and Diseases with 3D Radiative Transfer Modeling. *Remote Sens. Environ.* **2023**, *297*, 113759. [CrossRef]
20. Liu, W.; Atherton, J.; Mottus, M.; Gastellu-Etchegorry, J.-P.; Malenovsky, Z.; Raumonen, P.; Akerblom, M.; Makipaa, R.; Porcar-Castell, A. Simulating Solar-Induced Chlorophyll Fluorescence in a Boreal Forest Stand Reconstructed from Terrestrial Laser Scanning Measurements. *Remote Sens. Environ.* **2019**, *232*, 111274. [CrossRef]
21. Li, W.; Hu, X.; Su, Y.; Tao, S.; Ma, Q.; Guo, Q. A new method for voxel-based modelling of three-dimensional forest scenes with integration of terrestrial and airborne LiDAR data. *Methods Ecol. Evol.* **2024**, *15*, 569–582. [CrossRef]
22. Schneider, F.D.; Leiterer, R.; Morsdorf, F.; Gastellu-Etchegorry, J.-P.; Lauret, N.; Pfeifer, N.; Schaepman, M.E. Simulating Imaging Spectrometer Data: 3D Forest Modeling Based on LiDAR and in Situ Data. *Remote Sens. Environ.* **2014**, *152*, 235–250. [CrossRef]
23. Calders, K.; Origo, N.; Burt, A.; Disney, M.; Nightingale, J.; Raumonen, P.; Åkerblom, M.; Malhi, Y.; Lewis, P. Realistic Forest Stand Reconstruction from Terrestrial LiDAR for Radiative Transfer Modelling. *Remote Sens.* **2018**, *10*, 933. [CrossRef]
24. Janoutová, R.; Homolová, L.; Novotný, J.; Navrátilová, B.; Pikl, M.; Malenovský, Z. Detailed Reconstruction of Trees from Terrestrial Laser Scans for Remote Sensing and Radiative Transfer Modelling Applications. *In Silico Plants* **2021**, *3*, diab026. [CrossRef]
25. Widlowski, J.-L.; Côté, J.-F.; Béland, M. Abstract Tree Crowns in 3D Radiative Transfer Models: Impact on Simulated Open-Canopy Reflectances. *Remote Sens. Environ.* **2014**, *142*, 155–175. [CrossRef]
26. Li, W.; Guo, Q.; Tao, S.; Su, Y. VBRT: A novel voxel-based radiative transfer model for heterogeneous three-dimensional forest scenes. *Remote Sens. Environ.* **2018**, *206*, 318–335. [CrossRef]
27. Persson, H.J.; Ekström, M.; Ståhl, G. Quantify and Account for Field Reference Errors in Forest Remote Sensing Studies. *Remote Sens. Environ.* **2022**, *283*, 113302. [CrossRef]
28. Widlowski, J.-L.; Mio, C.; Disney, M.; Adams, J.; Andredakis, I.; Atzberger, C.; Brennan, J.; Busetto, L.; Chelle, M.; Ceccherini, G.; et al. The Fourth Phase of the Radiative Transfer Model Intercomparison (RAMI) Exercise: Actual Canopy Scenarios and Conformity Testing. *Remote Sens. Environ.* **2015**, *169*, 418–437. [CrossRef]
29. Wang, Y.; Kallel, A.; Yang, X.; Regaieg, O.; Lauret, N.; Guilleux, J.; Chavanon, E.; Gastellu-Etchegorry, J.-P. DART-Lux: An Unbiased and Rapid Monte Carlo Radiative Transfer Method for Simulating Remote Sensing Images. *Remote Sens. Environ.* **2022**, *274*, 112973. [CrossRef]
30. Luo, Y.; Xie, D.; Qi, J.; Zhou, K.; Yan, G.; Mu, X. LESS LiDAR: A full-waveform and discrete-return multispectral LiDAR simulator based on ray tracing algorithm. *Remote Sens.* **2023**, *15*, 4529. [CrossRef]
31. Zhou, K.; Xie, D.; Qi, J.; Zhang, Z.; Bo, X.; Yan, G.; Mu, X. Explicitly Reconstructing RAMI-V Scenes for Accurate 3-Dimensional Radiative Transfer Simulation Using the LESS Model. *J. Remote Sens.* **2023**, *3*, 0033. [CrossRef]
32. Qi, J.; Xie, D.; Guo, D.; Yan, G. A Large-Scale Emulation System for Realistic Three-Dimensional (3-D) Forest Simulation. *IEEE J. Sel. Top. Appl. Earth Obs. Remote Sens.* **2017**, *10*, 4834–4843. [CrossRef]
33. He, S.; Qi, J.; Wang, D.; Yan, K.; Huang, H. Estimation of Canopy Photon Recollision Probability from Airborne Laser Scanning. *Remote Sens. Environ.* **2024**, *311*, 114264. [CrossRef]
34. Zhang, W.; Qi, J.; Wan, P.; Wang, H.; Xie, D.; Wang, X.; Yan, G. An Easy-to-Use Airborne LiDAR Data Filtering Method Based on Cloth Simulation. *Remote Sens.* **2016**, *8*, 501. [CrossRef]
35. Edelsbrunner, H.; Mucke, E. Three-Dimensional Alpha Shapes. *ACM Trans. Graph.* **1994**, *13*, 43–72. [CrossRef]
36. Lin, X.; Li, A.; Bian, J.; Zhang, Z.; Lei, G.; Chen, L.; Qi, J. Reconstruction of a Large-Scale Realistic Three-Dimensional (3-D) Mountain Forest Scene for Radiative Transfer Simulations. *GISci. Remote Sens.* **2023**, *60*, 2261993. [CrossRef]
37. Gao, G.; Qi, J.; Lin, S.; Hu, R.; Huang, H. Estimating Plant Area Density of Individual Trees from Discrete Airborne Laser Scanning Data Using Intensity Information and Path Length Distribution. *Int. J. Appl. Earth Obs. Geoinf.* **2023**, *118*, 103281. [CrossRef]
38. Zhao, X.; Qi, J.; Jiang, J.; Liu, S.; Xu, H.; Lin, S.; Yu, Z.; Li, L.; Huang, H. Fine-Scale Retrieval of Leaf Chlorophyll Content Using a Semi-Empirically Accelerated 3D Radiative Transfer Model. *Int. J. Appl. Earth Obs. Geoinf.* **2024**, *135*, 104285. [CrossRef]
39. Chen, S.; Liu, L.; Zhang, X.; Liu, X.; Chen, X.; Qian, X.; Xu, Y.; Xie, D. Retrieval of the Fraction of Radiation Absorbed by Photosynthetic Components (FAPARgreen) for Forest Using a Triple-Source Leaf-Wood-Soil Layer Approach. *Remote Sens.* **2019**, *11*, 2471. [CrossRef]
40. Wilson, R.T. Py6S: A Python Interface to the 6S Radiative Transfer Model. *Comput. Geosci.* **2013**, *51*, 166–171. [CrossRef]
41. Duursma, R.A.; Falster, D.S.; Valladares, F.; Sterck, F.J.; Pearcy, R.W.; Lusk, C.H.; Sendall, K.M.; Nordenstahl, M.; Houter, N.C.; Atwell, B.J.; et al. Light Interception Efficiency Explained by Two Simple Variables: A Test Using a Diversity of Small- to Medium-Sized Woody Plants. *New Phytol.* **2012**, *193*, 397–408. [CrossRef]
42. Plaga, B.N.E.; Bauhus, J.; Pretzsch, H.; Pereira, M.G.; Forrester, D.I. Influence of Crown and Canopy Structure on Light Absorption, Light Use Efficiency, and Growth in Mixed and Pure Pseudotsuga Menziesii and Fagus Sylvatica Forests. *Eur. J. For. Res.* **2024**, *143*, 479–491. [CrossRef]

43. Li, Y.; Su, Y.; Hu, T.; Xu, G.; Guo, Q. Retrieving 2-D Leaf Angle Distributions for Deciduous Trees from Terrestrial Laser Scanner Data. *IEEE Trans. Geosci. Remote Sens.* **2018**, *56*, 4945–4955. [CrossRef]
44. Ando, R.; Ozasa, Y.; Guo, W. Robust Surface Reconstruction of Plant Leaves from 3D Point Clouds. *Plant Phenomics* **2021**, *2021*, 3184185. [CrossRef] [PubMed]
45. Cai, S.; Zhang, W.; Zhang, S.; Yu, S.; Liang, X. Branch architecture quantification of large-scale coniferous forest plots using UAV-LiDAR data. *Remote Sens. Environ.* **2024**, *306*, 114121. [CrossRef]

Disclaimer/Publisher's Note: The statements, opinions and data contained in all publications are solely those of the individual author(s) and contributor(s) and not of MDPI and/or the editor(s). MDPI and/or the editor(s) disclaim responsibility for any injury to people or property resulting from any ideas, methods, instructions or products referred to in the content.